Fast-slow wave transitions induced by a random mean flow

S. Boury ⊙,* O. Bühler ⊙, and J. Shatah
Courant Institute of Mathematical Sciences, New York University, New York, New York 10012, USA

Motivated by recent asymptotic results in atmosphere-ocean fluid dynamics, we present an idealized numerical and theoretical study of two-dimensional dispersive waves propagating through a small-amplitude random mean flow. The objective is to delineate clearly the conditions under which the cumulative Doppler shifting and refraction by the mean flow can change the group velocity of the waves not only in direction, but also in magnitude. The latter effect enables a possible transition from fast to slow waves, which behave very differently. Within our model we find the conditions on the dispersion relation and the mean flow amplitude that allow or rule out such fast-slow transitions. For steady mean flows we determine a finite mean flow amplitude threshold below which such transitions can be ruled out indefinitely. For unsteady mean flows a sufficiently rapid rate of change means that this threshold goes to zero, i.e., in this scenario all waves eventually undergo a fast-slow transition regardless of mean flow amplitude, with corresponding implications for the long-term fate of these waves.

I. INTRODUCTION

Nonlinear interactions between waves and nonuniform mean flows have been recognized as important in atmosphere-ocean fluid dynamics since the 1960s. Prominent examples include the driving of long-shore currents by surface waves [1], or the driving of the meridional circulation in the middle atmosphere by internal gravity and Rossby waves [2]. Much of the early work was based on monochromatic waves encountering critical layers induced by large-amplitude steady shear flows [3], but since then theory and simulations have extended these concepts in many ways (e.g., see the textbooks [4,5]).

Recently, the cumulative impact of wave refraction due to a small-amplitude random mean flow has been investigated in a number of geophysical settings by building on classical scattering theory for sound or light waves in random media (e.g., Refs. [6–9]). This is most easily studied by assuming a scale separation between waves and mean flows, which allows the use of well-established ray-tracing techniques for slowly varying wave trains. (This is a relevant though by no means universally valid assumption in atmosphere-ocean dynamics, and some recent scattering studies have gone beyond that assumption.) However, geophysical waves are strongly dispersive and thus can behave in ways that are not possible for sound or light waves. Most importantly, the group velocity of such waves can transform significantly not only in direction but also in magnitude, for instance turning fast waves into slow waves in a manner to be defined precisely below, and this inevitably has important consequences for the long-term evolution of the waves (e.g., one may recall that at a critical layer the group velocity goes to zero).

The present study combines detailed ray-tracing simulations with idealized theory to investigate such fast-slow transitions in a two-dimensional model for dispersive waves exposed to a random mean flow. This setup allows us to delineate clearly under what *a priori* conditions on the dispersion relation and mean flow amplitude the waves may or may not undergo a fast-slow transition. We also demonstrate the vivid differences between fast and slow wave evolution, such as the trapping of slow waves in coherent vortices.

II. RAY TRACING FOR DISPERSIVE WAVES ON MEAN FLOWS

In a slowly varying wave train the wave action density A is defined as the wave energy density E divided by the local intrinsic frequency ω, i.e., $A = E/\omega$. It is the domain-integrated wave action, and not the wave energy, that is then conserved even in the presence of a slowly varying mean flow **U** [10]. In the special case of a wave packet this implies conservation of packet-integrated wave action along the wave packet trajectories, or rays. Changes in the wave packet energy $E = \omega A$ are then proportional to changes in ω along the rays, so changes in ω are of particular relevance in wave-mean interactions. Both the wave packet dynamics and the wave action conservation are neatly summarized in a Liouville equation

$$\partial_t A + \nabla_{\mathbf{k}}\Omega \cdot \nabla_{\mathbf{x}}A - \nabla_{\mathbf{x}}\Omega \cdot \nabla_{\mathbf{k}}A = 0 \tag{1}$$

for the wave action density in phase space $A(\mathbf{x}, \mathbf{k}, t)$. Here **k** is the wave-number vector and the action density in real space is the integral of A over **k**. This allows for the incoherent superposition of different wave packets at the same location, which is an advantage in many practical applications [11]. The characteristics of (1) are the wave packet rays

$$[\dot{\mathbf{x}}(t), \dot{\mathbf{k}}(t)] = (\nabla_{\mathbf{k}}, -\nabla_{\mathbf{x}})\Omega(\mathbf{x}, \mathbf{k}, t) \tag{2}$$

in phase space. The absolute frequency Ω acts as a Hamiltonian function for the phase space flow in (2). In general, Ω is the sum of the usual intrinsic frequency ω plus a

---

*sb7918@nyu.edu

055101-1

Doppler-shifting term involving the mean flow

$$\Omega(\mathbf{x}, \mathbf{k}, t) = \omega(\mathbf{k}) + \mathbf{U}(\mathbf{x}, \mathbf{t}) \cdot \mathbf{k}. \qquad (3)$$

Physically, Ω is the frequency observed in a reference frame at rest and ω is the frequency observed in a reference frame moving with the local velocity $\mathbf{U}$. In general, ω may depend on $\mathbf{x}$ and t as well, but we restrict to $\omega(\mathbf{k})$ in our study. The absolute group velocity is $\nabla_{\mathbf{k}}\Omega = \mathbf{c_g} + \mathbf{U}$ where $\mathbf{c_g} = \nabla_{\mathbf{k}}\omega$ is the intrinsic group velocity. So the wave packet is advected by the mean flow and also moves relative to it with $\mathbf{c_g}$. The key dynamical process in (2) and (3) is the refraction of $\mathbf{k}$ by the variable mean flow, i.e., $\dot{\mathbf{k}} = -(\nabla_{\mathbf{x}}\mathbf{U}) \cdot \mathbf{k}$. Notably, in the important special case of a steady flow $\mathbf{U}(\mathbf{x})$, the Hamiltonian function $\Omega(\mathbf{x}, \mathbf{k})$ has no explicit time dependence and hence, despite refraction, the value of Ω is constant along a ray. This provides some forever memory of the wave packet's initial conditions, which will be shown to be important below.

A. Fast and slow waves

Fast and slow waves are distinguished based on the relative magnitude of $\mathbf{c_g}$ vs. $\mathbf{U}$. For slow waves $|\mathbf{c_g}| \ll |\mathbf{U}|$ holds and therefore advection by the mean flow dominates the wave propagation, which implies that slow wave rays closely resemble particle trajectories. Indeed, in the limiting case where $\mathbf{c_g}$ is completely negligible in (2), we have $\Omega \approx \mathbf{U} \cdot \mathbf{k}$ and the evolution of $\mathbf{k}(t)$ becomes identical to that of the gradient of a passive scalar. This limiting regime was explored in detail for internal gravity waves in Ref. [12].

Alternatively, for fast waves $|\mathbf{c_g}| \gg |\mathbf{U}|$ holds, which is evidently relevant for light or sound waves, but also for surface waves relative to the typical current speeds in the ocean. To first approximation the waves are then unaffected by the mean current and simply travel along straight lines while maintaining constant $\mathbf{k}$. Meaningful interaction effects accrue slowly over long propagation times, which makes their study amenable to asymptotic analysis based on a small parameter such as

$$\varepsilon_0 = \frac{U_0}{c_{g0}} \ll 1. \qquad (4)$$

Here U_0 is the typical amplitude of $|\mathbf{U}|$ and $c_{g0} = |\mathbf{c_g}(0)|$ is the initial group velocity [7,13,14]. The Doppler-shifting term is then small in (3) and therefore $\Omega \approx \omega$. Crucially, for a steady mean flow the exact invariance of Ω then implies the approximate invariance of ω along a ray. Wave action conservation then implies wave energy conservation even in the presence of a mean flow, which severely limits the interactions between the waves and the mean flow.

This was exploited by asymptotic analysis and numerical simulation in a study of three-dimensional (3D) internal gravity waves by Kafiabad *et al.* [7]. Building on the earlier work of McComas and Bretherton [15] and Ryzhik *et al.* [16], these authors modeled $\mathbf{U}$ as a steady random mean flow with homogeneous statistics and this allowed them to derive a diffusion approximation to (1) of the form

$$\partial_t A + \mathbf{c_g} \cdot \nabla_{\mathbf{x}} A = \nabla_{\mathbf{k}} \cdot (\mathbf{D} \cdot \nabla_{\mathbf{k}} A), \qquad (5)$$

where, for internal waves,

$$\omega = \sqrt{N^2 \frac{|\mathbf{k_\perp}|^2}{|\mathbf{k}|^2} + f^2 \frac{|\mathbf{k_z}|^2}{|\mathbf{k}|^2}} \Rightarrow c_g = |\mathbf{c_g}| \propto \frac{1}{|\mathbf{k}|}, \qquad (6)$$

with $\mathbf{k_\perp}$ the horizontal component of the wave vector, $\mathbf{k_z}$ its vertical component, and N and f the Brunt-Väisälä and the Coriolis frequencies, respectively.

Here, $\mathbf{D}$ is a symmetric $O(\varepsilon_0^2)$ diffusion matrix that describes the scattering in wave number space due to refraction by the mean flow. The details of $\mathbf{D}$ depend on the power spectrum of the mean flow, but for all steady mean flows $\mathbf{D}$ has the property that the diffusive flux $\mathbf{D} \cdot \nabla_{\mathbf{k}} A$ is always perpendicular to the surfaces of constant ω in three-dimensional wave number space. In other words, there is diffusion along surfaces of constant ω, but none across them. This recovers the approximate conservation of ω alluded to before. Recently, this study has been extended to include weakly time-dependent $\mathbf{U}$, which did not change the results significantly [8]. The frequency of internal waves depends only on the angle that $\mathbf{k}$ makes with the vertical, so the diffusion takes place along unbounded cones in three-dimensional $\mathbf{k}$ space and this allows $k = |\mathbf{k}|$ to grow without bound even at constant ω.

The situation is somewhat different in two-dimensional cases of geophysical interest. For example, Villas, Boas, and Young [6] adapted Kafiabad *et al.* [7] to the case of deep-water surface waves, where $\omega = \sqrt{gk}$ with gravity g. Now the contours of constant ω in two-dimensional $\mathbf{k}$ space are circles around the origin, so constant ω implies constant k and therefore the diffusion takes place on a bounded manifold. For isotropic two-dimensional wave systems the diffusion previously introduced is therefore only angular: the wave vector $\mathbf{k}$ keeps a constant magnitude, and the diffusion only acts on its orientation.

In this situation the assumption of a steady mean flow $\mathbf{U}(\mathbf{x})$ is in fact crucial for the long-term development of $\mathbf{k}$. This was demonstrated by Dong *et al.* [17] in a ray-tracing study of rotating shallow water gravity waves exposed to steady and unsteady random mean currents. Here the isotropic dispersion relation is $\omega = \sqrt{f^2 + gHk^2}$ with Coriolis parameter f and undisturbed layer depth H. For steady flows with small Froude number $F = U_0/\sqrt{gH} \ll 1$ it follows that ω can drift from its initial value only by an $O(F)$ amount and this bound is valid uniformly in time. However, this changes completely for unsteady mean flows $\mathbf{U}(\mathbf{x}, t)$, which breaks the forever memory and allows Ω and therefore ω to drift away from their initial values. A robust evolution toward increased values of ω was then observed numerically, which meant the waves robustly extracted energy from the mean flow.

B. Fast-slow transitions

Whether transitions between fast and slow wave regimes are possible depends foremost on the specifics of the dispersion relation $\omega(\mathbf{k})$. For example, in the aforementioned studies of internal gravity waves both regimes were possible for oceanic conditions, so a transition from fast to slow internal waves is of particular interest both from a theoretical and a practical perspective. This prompted a detailed ray-tracing study for three-dimensional internal gravity waves reported in

Ref. [14], in which all wave packets start out as fast in the sense of $\varepsilon_0 \ll 1$. Surprisingly, it was found that even steady mean flows already induced a fairly rapid fast-slow transition along the wave rays. Indeed, this led to the spontaneous generation of a broadband spectrum in ω, in seeming contradiction with the constant-ω prediction of the diffusion theory based on $\varepsilon_0 \ll 1$. These numerical results can be reconciled with the diffusion theory upon noting that that theory is not uniformly valid in time, i.e., its validity is restricted $O(\varepsilon_0^{-2})$ time and length scales. The observed fast-slow transition occurred after an initial phase that was indeed well described by the diffusion theory.

The mechanism for this dramatic departure from the constant-ω regime is easy to understand in principle. For internal waves the group velocity at fixed frequency is proportional to k^{-1}, a fact that can be corroborated either by direct calculation or by observing that for these waves $\omega(\mathbf{k})$ is homogeneous of degree zero in $\mathbf{k}$ and therefore $\mathbf{c_g} = \nabla_{\mathbf{k}}\omega$ must be homogeneous of degree minus one in $\mathbf{k}$ [5]. In general, wave refraction by mean-flow shear and strain has a tendency to shorten the wavelength and therefore to increase k, which for internal waves means that c_g decreases along a ray. Hence a ray may start with large c_{g0} compared to U_0 but then c_g decreases substantially, making both speeds comparable, or even leading to the wave-capturing regime discussed in Ref. [12], which is characterized by $c_g \ll U_0$.

The fast-slow transition marks the departure from the constant-ω dynamics described by the diffusion equation and opens the door to strong wave-mean interactions, in which significant energy can be exchanged between the waves and the mean flow. Conversely, for some wave systems the reverse transition can also take place, i.e., slow waves may turn into fast waves.

We investigate this via simple theory and detailed numerical simulations of idealized two-dimensional wave packets based on a dispersion relation that is isotropic in $\mathbf{k} = (k_x, k_y)$ and involves an adjustable power-law exponent α

$$\omega(k) = \begin{cases} \frac{1}{\alpha}k^{\alpha}, & \alpha \neq 0 \\ \log(k), & \alpha = 0, \end{cases} \tag{7}$$

yielding

$$\mathbf{c_g} = k^{\alpha-2}\,\mathbf{k}, \quad c_g = |\mathbf{c_g}| = k^{\alpha-1}. \tag{8}$$

This family includes as special cases nondispersive waves ($\alpha = 1$), deep-water waves ($\alpha = 1/2$), and quantum-mechanical matter waves ($\alpha = 2$). If $|\alpha| \ll 1$ it also mimics the aforementioned $c_g \propto 1/k$ scaling behavior of internal waves. The singular limit $\alpha \to 0$, corresponding to a group velocity $c_g = k^{-1}$ as in the case of internal waves, is regularized numerically by using the dispersion relation $\omega(k) = \log(k)$. Of course, this simple two-dimensional model differs from three-dimensional internal waves in other respects. Most importantly, perhaps, is that in our model the sets of wave numbers sharing the same intrinsic frequency are circles and therefore bounded, whereas for internal waves they are cones and therefore unbounded.

The wave packets propagate through a nondivergent mean flow $\mathbf{U}$ modeled as a Gaussian random function with homogeneous and isotropic statistics. For most simulations $\mathbf{U}$ is steady, but an unsteady case with stationary statistics is

also considered in Sec. V. A large number of ray-tracing experiments are then performed to extract the statistics of the wave behavior. These experiments together with some simple theory then answer two questions: first, for what dispersion relations is either the slow or the fast wave regime the only long-time attractor? And second, are there dispersion relations that allow both regimes to be long-time attractors, so that the ultimate behavior depends forever on the initial conditions?

III. NUMERICAL METHODS

We scale the mean flow explicitly as $\varepsilon_0 \mathbf{U}$ and therefore (2) and (3) become

$$\dot{\mathbf{x}}(t) = \nabla_{\mathbf{k}}\Omega = \mathbf{c_g} + \varepsilon_0\mathbf{U} \tag{9}$$

$$\dot{\mathbf{k}}(t) = -\nabla_{\mathbf{x}}\Omega = -\varepsilon_0(\nabla_{\mathbf{x}}\mathbf{U})\cdot\mathbf{k} \tag{10}$$

and

$$\Omega = \omega(k) + \varepsilon_0\mathbf{U}\cdot\mathbf{k}. \tag{11}$$

Here $\mathbf{U}$ is normalized such that its root-mean-square value (RMS) is equal to unity, i.e., $U_0 = 1$. The starting locations of the rays are chosen deterministically on a uniform grid and the initial direction of $\mathbf{k}$ is chosen randomly for each ray. All waves start with $k_0 = 1$ and therefore $c_{g0} = 1$ from (7). As an aside, it is easy to check that for steady $\mathbf{U}(\mathbf{x})$ the choice $k_0 = 1$ does not limit the generality of our setup, as any other choice can be rescaled to this one. However, this is not true for unsteady $\mathbf{U}(\mathbf{x}, t)$. As the wave packets evolve the ratio of mean flow to group velocity is monitored along rays (with a slight abuse of notation) as

$$\varepsilon(t) = \varepsilon_0\frac{|\mathbf{U}|}{|\mathbf{c_g}|}. \tag{12}$$

Hence $\varepsilon(0) \approx \varepsilon_0$ and a fast-slow transition corresponds to $\varepsilon(t)$ reaching large values even though $\varepsilon_0 \ll 1$.

The steady mean flow derives from a stream function ψ as

$$\mathbf{U}(\mathbf{x}) = (-\partial_y\psi, \partial_x\psi), \tag{13}$$

where $\psi(\mathbf{x})$ is modeled as a zero-mean Gaussian random function with isotropic and homogeneous covariance function. This is realized as best as possible in a doubly periodic domain by choosing the Fourier coefficients of ψ as independent random variables drawn from a zero-mean normal distribution. Explicitly, the Fourier coefficients are

$$\hat{\psi} = \frac{1}{q}\sqrt{\frac{C}{2}q^{-n-1}}\,(a+ib), \tag{14}$$

where q is the magnitude of the wave number of the Fourier component, (a, b) are independent standard normal variables for each Fourier component, and C a normalization constant that ensures that the RMS of $\mathbf{U}$ is $U_0 = 1$. Only a finite band of wave numbers between $q_{\min} = 1$ and $q_{\max} = 30$ is allowed and care is taken to ensure the reality condition. Setting $q_{\min} > 0$, ensures that the mean value of the mean flow is 0. The parameter $n > 0$ sets the slope of the one-dimensional kinetic energy spectrum to q^{-n}.

We generated two sets of ten mean flows that we used throughout the study, with $n = 3$ (corresponding to the direct, enstrophy cascade of 2D turbulence) and $n = 5/3$ (corresponding to the inverse, energy cascade in the same situation).
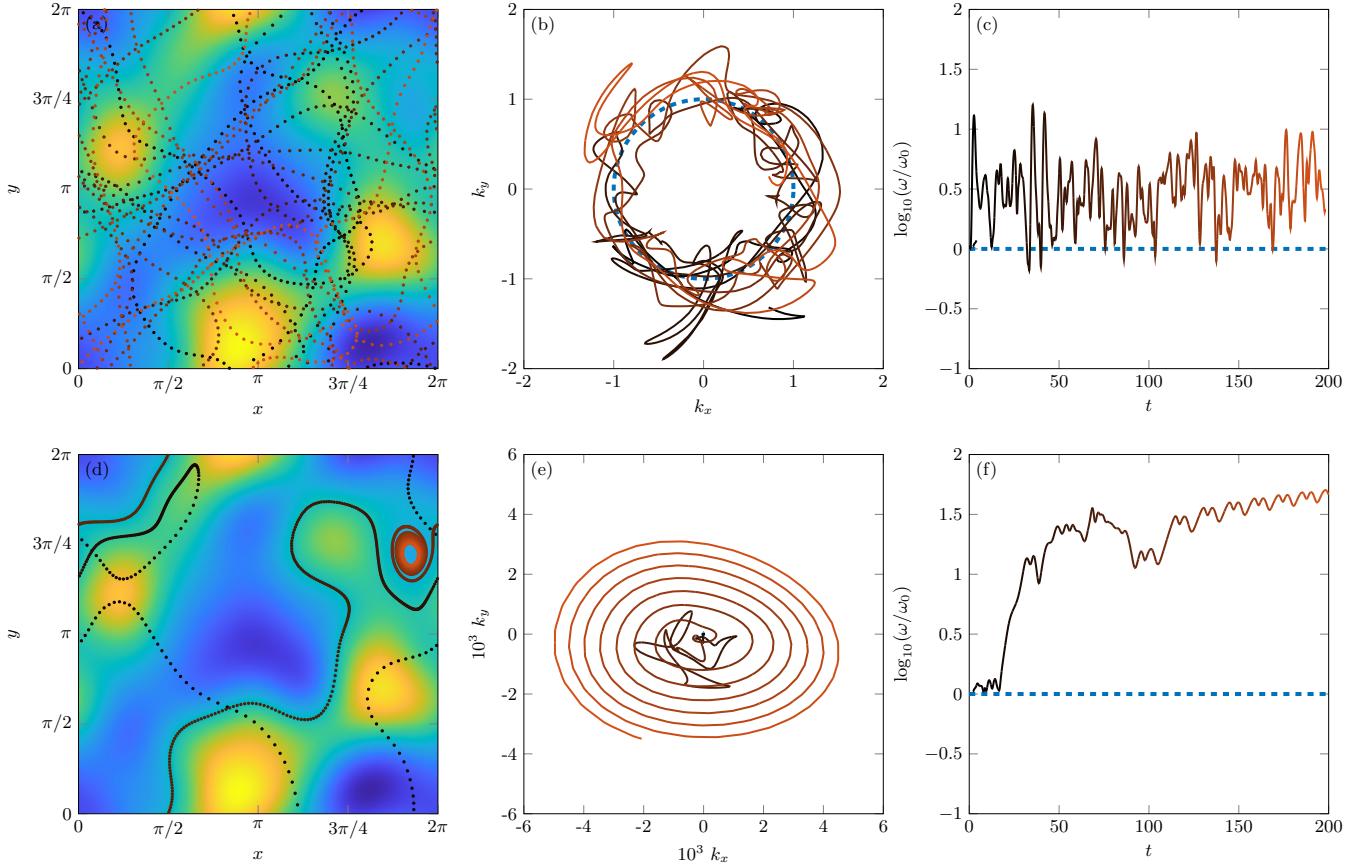
FIG. 1. Sample rays in two cases. The first column shows the ray path as dots in physical space, superimposed on the stream function of the mean flow; the spacing of the dots becomes denser and resembles a solid line if the ray slows down. Lighter red color refers to later times for orientation. The second column shows the path of the ray in the phase space and the third column shows the logarithm of the intrinsic frequency ω as a function of time. Top row: $\alpha = 1.2$ and $\varepsilon_0 = 0.5$, corresponding to an ergodic trajectory with no shift in frequency and no fast-slow transition. Bottom row: $\alpha = 0.5$ and $\varepsilon_0 = 0.5$, corresponding to a trapped trajectory with shift in frequency, indicative of the fast-slow transition.

The flows are defined on a $2\pi \times 2\pi$ doubly periodic domain, with 512×512 grid points. These values ensured numerical convergence, but our results remained qualitatively insensitive to decreasing or increasing the grid resolution.

The Hamiltonian ray-tracing system is then solved numerically using MATLAB's ODE45 scheme with adaptive time stepping, and relative and absolute tolerances were set to 10^{-3}. The random mean flow and its gradient tensor is computed exactly from the Fourier modes at each grid position and then interpolated to the wave packet positions using linear interpolation from the closest neighbors. The accuracy of this interpolation step is the most important element of the numerical scheme for the purpose of accurate computation of the ray paths. We checked that changing the error tolerances to 10^{-2} and to 10^{-4} did not change the results, although the effort required to compute a large number of rays with a tolerance down to 10^{-4} is then significantly increased, due to the adaptative time stepping.

IV. RESULTS FOR STEADY MEAN FLOWS

Throughout this section we consider a random steady mean flow of the form (14) with power law $n = 3$. For a steady mean flow the invariance of Ω along rays implies that changes

in $\omega(k)$ are compensated by changes in the Doppler-shifting term $\varepsilon_0 \mathbf{U} \cdot \mathbf{k}$. In the regime $\alpha > 1$ changes with k are superlinear in ω but only linear in the Doppler-shifting term, hence the stretching of $\mathbf{k}$ must eventually cease because the aforementioned compensation becomes impossible. Together with the increase of c_g with k if $\alpha > 1$, this leads to the simple prediction that in this regime fast waves remain fast forever, i.e., that $\varepsilon_0 \ll 1$ implies $\varepsilon(t) \ll 1$ uniformly in t. Moreover, it also appears likely that almost all slow waves will eventually transition to fast waves, simply because any stretching of $\mathbf{k}$ will reduce $\varepsilon(t)$.

Conversely, if $\alpha < 1$ then the dynamics is reversed: the frequency changes sublinearly with k, making the changes in the Doppler-shifting term dominant, and c_g decreases as $\mathbf{k}$ is stretched. This suggests that in this regime slow waves remain slow, while fast waves may also transition to slow waves.

A. Ergodic and trapped rays

The qualitative difference between these two regimes is illustrated with a couple of sample runs in Fig. 1. Both runs start with $\varepsilon_0 = 0.5$ but in the first run $\alpha = 1.2$ whereas in the second it is $\alpha = 0.5$. As expected, in the first run the wave remains fast, traverses the domain in a seemingly ergodic
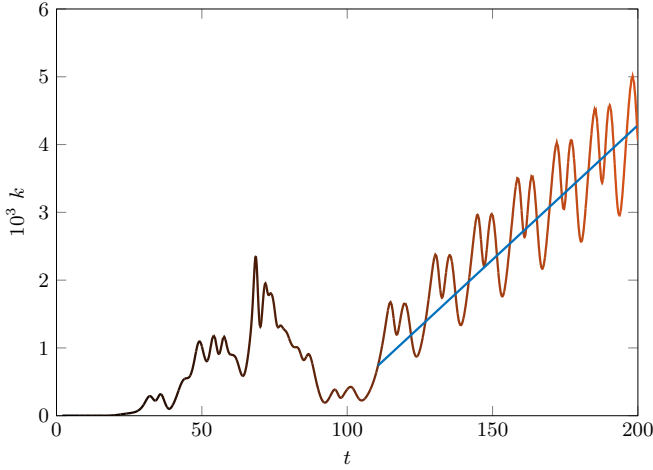
FIG. 2. Evolution of k in the case $\alpha = 0.5$ and $\varepsilon_0 = 0.5$. The wave packet is trapped around $t \approx 100$ and afterwards k exhibits secular growth, with fluctuations around a linear trend (oblique blue line).

fashion, and there is no discernible trend in k/k_0 or ω/ω_0. By contrast, in the second run there is a fast-slow transition, k/k_0 and ω/ω_0 sharply increase, and the ray gets trapped in a single vortex.

As an aside, in the second case k eventually grows linearly in time once the wave has been trapped. This can be explained by considering the limiting dynamics of passive advection by a circumferential vortex flow $U(r)$, say. The wave packet maintains a fixed radius r and its angular momentum is conserved, so

$$\dot{r} = 0 \quad \text{and} \quad (\mathbf{k} \times \mathbf{r})^{\cdot} = \mathbf{0}. \tag{15}$$

With $\mathbf{k} = (k_r, k_\theta)$ it follows that $\dot{k}_\theta = 0$ and, using Eq. (10), that

$$\dot{k}_r = -rk_\theta \frac{\mathrm{d}}{\mathrm{d}r}\left(\frac{U(r)}{r}\right). \tag{16}$$

This makes obvious that any nonuniform angular velocity U/r eventually leads to secular growth of k_r and k. Indeed, Fig. 2 shows k in the $\alpha = 0.5$ case of Fig. 1: the blue line shows the mean trend when the ray is trapped, corroborating this simple explanation.

The two different regimes can be explored statistically by looking at the sample distribution at $t = 200$ of 1600 rays initially distributed evenly on a 40×40 grid. The outcome is shown in Fig. 3 with $\alpha = 1.2$ and $\varepsilon_0 = 0.5$ at the top and $\alpha = 0.5$ and $\varepsilon_0 = 0.5$ at the bottom (same values as in Fig. 1). The left plots present the end locations of the rays superimposed on the stream function and the center plots coarse grains this distribution over 20×20 bins to estimate the probability density function (PDF) of the rays. This makes the concentration of rays in the vortex cores qualitatively apparent in the $\alpha = 0.5$ case. To measure this quantitatively we exploit that the stream function ψ is negatively correlated with the vorticity $\nabla^2 \psi$ and therefore $|\psi|$ is positively correlated with the vorticity magnitude. Hence $|\psi|$ can be used as a smooth proxy for vortex cores and the third column shows the time evolution of the sample Pearson correlation coefficient $R(t)$

between $|\psi|$ and the ray PDF. In the $\alpha > 1$ regime R fluctuates close to zero, but in the $\alpha < 1$ regime R rises to 0.3 and stays at this value for the entire time of the simulations. These results are insensitive to the particular mean flow sample being used.

B. Phase diagram of fast-slow transitions

We perform a large number of simulations to map out the long-term behavior of the rays as a function of the parameters α and ε_0, which yields a phase diagram of the fast-slow transitions. We discretize in steps of 0.025 in either parameter and choose limits of $\alpha = -2.4$ through 1.2 and $\varepsilon_0 = 0.025$ through 1. The asymmetric range of α focuses on the potential trapping regime with $\alpha < 1$. For each (α, ε_0) we draw ten random mean flow samples and launch 16 rays spaced on a uniform grid for each sample, corresponding to a total of 160 rays for each location in phase space. The evolution of the intrinsic ω and ε are monitored as a function of time and averaged over all rays.

The phase diagram of the values of ε at $t = 200$ is presented in Fig. 4 for two different mean flows. Both have $q_{min} = 1$ and $q_{max} = 30$ but their power-law exponent is different: $n = 3$ in the top row and $n = 5/3$ in the bottom row. The center plots show the corresponding phase diagram with the ray-averaged $\varepsilon(200)$ color shaded such that blue corresponds to fast waves and red to slow waves. We identify two regimes: (i) a slow regime in which $\varepsilon(t)$ goes to high values (saturation of the color bar in red), indicating that the group velocity becomes small compared to the mean flow; and (ii) a fast regime in which $\varepsilon(t)$ remains bounded and smaller than 1. As discussed in the case of a single ray, these regimes are associated with (i) a significant shift in intrinsic frequency or (ii) no such shift and therefore ω remains close to its initial value. In the shift case, not all rays are trapped in background flow structures but the system reaches a state in which a majority of rays are trapped. Moreover, some rays can still escape this trapped dynamics while others are being trapped in turn; we observed that this detrapping behavior is more likely to occur close to the regime boundary. On the other hand, none of the rays are trapped in the no-shift case, their trajectory being ergodic.

As previously mentioned, a clear boundary at $\alpha = 1$ is seen when ε_0 approaches 1, highlighted by a white dashed line; this boundary has been detected consistently in other runs for values of ε_0 up to 1.5. For $\alpha > 1$, no fast-slow transitions have been detected in the simulations and the only attracting end state is the fast wave regime. For $\alpha < 1$, however, there is a threshold for ε_0 such that above the threshold the slow wave regime now becomes the only attracting state (identified in Fig. 4, right). Conversely, below that threshold the fast wave regime remained the attractor for the duration of the integration. We found very little sensitivity of these threshold values to integration time and domain size, which warrants a closer inspection of the dynamics near these values.

C. Threshold Boundary

The existence of a threshold in ε_0 below which a fast-slow transition becomes impossible can be made plausible by considering the detailed consequences of the conservation
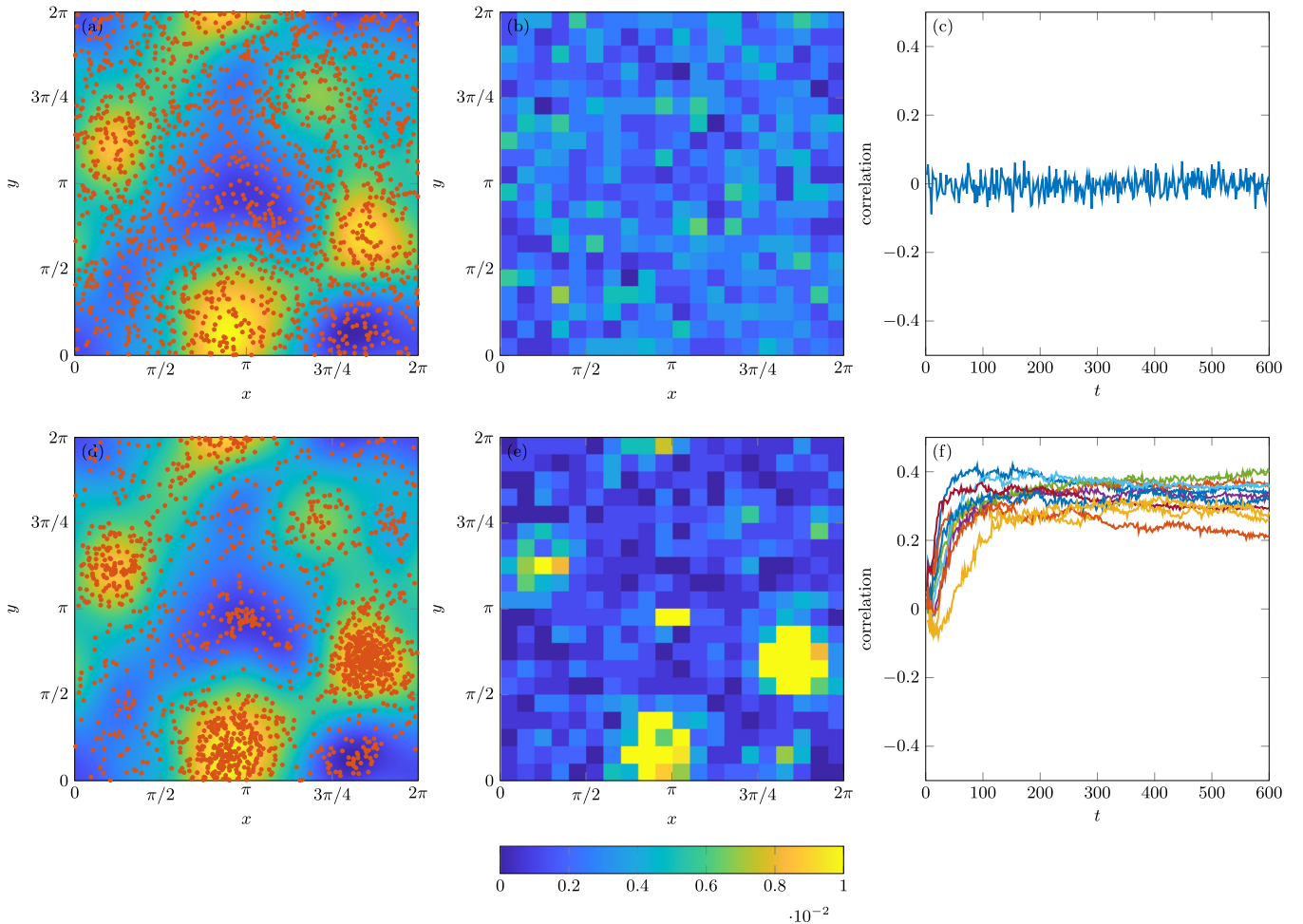
FIG. 3. Top row: no-transition case with $\alpha = 1.2$ and $\varepsilon_0 = 0.5$. Bottom row: fast-slow transition case with $\alpha = 0.5$ and $\varepsilon_0 = 0.5$. Left: stream function ψ and 1600 rays at $t = 200$. Center: normalized PDF computed by counting the rays on a coarse-grained grid. Right: sample correlation coefficient between $|\psi|$ and the ray PDFs, which is close to zero in the no-transition case but significantly positive in the fast-slow transition case (several graphs for different mean flow samples are plotted).

of absolute frequency in (3) for the illustrative case $\alpha = 1/2$, which is relevant to the deep-water surface waves studied in Ref. [6]. For $\alpha = 1/2$ the conservation law $\Omega = \Omega_0$ is

$$2\sqrt{k} + \varepsilon_0 U k \cos\theta = \frac{1}{\alpha}\sqrt{k_0} = 2. \qquad (17)$$

Here $U = |\mathbf{U}|$, θ is the angle between $\mathbf{U}$ and $\mathbf{k}$, and the initial Doppler-shifting term has been neglected for simplicity. This is a quadratic equation for $\sqrt{k}$ and for small ε_0 its roots are $O(1)$ on one branch and $O(1/\varepsilon_0)$ on the other. The ray starts with $\sqrt{k_0} = 1$ on the $O(1)$ branch and a fast-slow transition corresponds to a continuous transition to the other, $O(1/\varepsilon_0)$ branch. This requires that the two branches coincide on a double root, the condition for which is that

$$1 + 2\varepsilon_0 U \cos\theta = 0 \qquad (18)$$

holds at some moment in time along the ray. If ε_0 is small enough that this condition can never be satisfied then a fast–slow transition is strictly impossible. For a single flow sample a strict threshold for ε_0 can be computed from this condition using the maximum flow velocity of the sample. For random mean flows the threshold depends on the extreme-value

statistics of the flow, e.g., for a two-dimensional Gaussian random mean flow with unit variance a restriction to flow speeds within three standard deviations yields $|U \cos\theta| \leqslant 3/\sqrt{2}$, so $\varepsilon_0 < \sqrt{2}/6 \approx 0.24$ would be a reasonable threshold for this random mean flow. This agrees quite well with the observed threshold for $\alpha = 1/2$ in Fig. 4. Notably, the relevant ε_0 values for the surface waves studied in Ref. [6] were significantly below this threshold, which is the consistent with the lack of fast-slow transitions observed in that study. The case $\alpha = -1$ also leads to a quadratic equation, which then yields the threshold $\varepsilon_0 < \sqrt{2}/12 \approx 0.12$, again in good agreement with Fig. 4. We were not able to derive a general formula for the threshold as a continuous function of $\alpha < 1$. Some heuristic arguments suggest that the threshold is proportional to $1/(1 - \alpha)$, which appears broadly consistent with the numerical results, but is not very accurate when comparing the detailed results for the two cases $\alpha = 1/2$ and $\alpha = -1$.

The threshold boundary converges towards a similar shape for different random mean flows: in Fig. 4, we present the results for mean flows with power laws $n = 3$ and $n = 5/3$, but we also observed it for various other cases such as $n = 2$ or $n = 10$. For example, the threshold at $\alpha = 0$ varied slightly
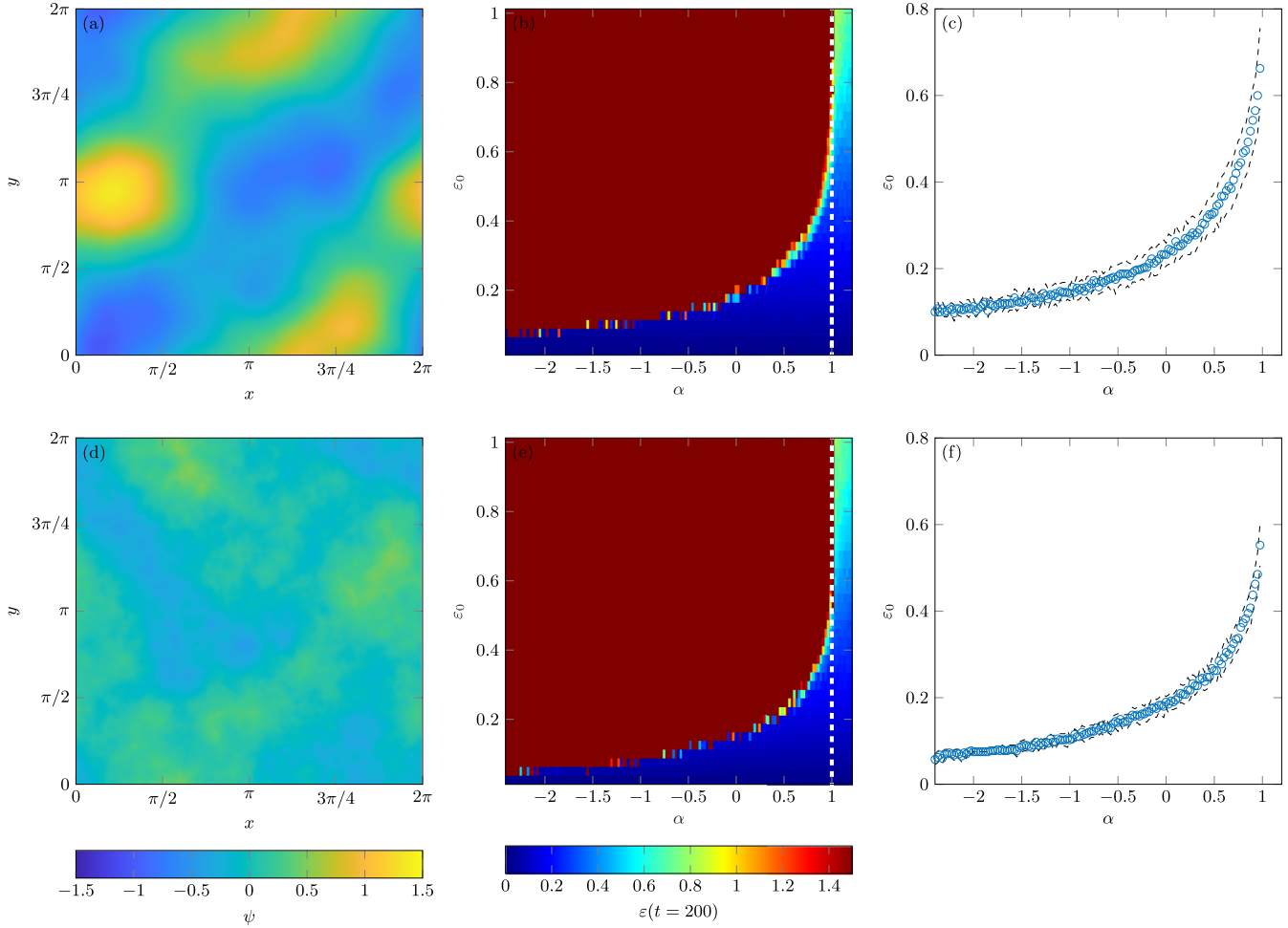
FIG. 4. Comparison between the $n = 3$ case (top row) and the $n = 5/3$ case (bottom row), showing a representative stream function (left), the phase diagram of $\varepsilon(t = 200)$ in the (α, ε_0) space obtained by computing the trajectories of 16 rays on ten mean flows (center), and the extracted mean boundary with its standard deviation computed over the ten mean flows (right).

but was always in the range 0.2 ± 0.05. This convergence is also very robust, as the boundary can be obtained only with statistics on a few set of rays (9 rays for a single mean flow, for instance, would give qualitatively the same behavior as the 160 rays used to obtain Fig. 4).

V. UNSTEADY MEAN FLOWS

Based on the earlier work on two-dimensional ray dynamics in Ref. [17] it can be anticipated that allowing the mean flow to be time dependent will have a significant impact on the fast-slow transitions. We explored this by using a simple stochastic model for the time evolution of the Fourier coefficients in (14). Specifically, all the parameters (a, b) undergo independent Ornstein-Uhlenbeck processes (e.g., Ref. [18]) with unit variance and temporal autocorrelation that decays exponentially with an adjustable decay rate $\gamma \geqslant 0$. This produces a time-dependent mean flow with stationary statistics and $\gamma = 0$ recovers the steady mean flow from before. In actual fluid dynamics the autocorrelation decay rate is a modest multiple of the vortex turnover rate, which scales as the vorticity $\varepsilon_0 \nabla^2 \psi$ in our model. Hence the most relevant

parameter range for γ is a modest fraction of the RMS vorticity, which we denote by $\varepsilon_0 \xi_0$, where ξ_0 is the unscaled RMS of the vorticity of the flow.

Phase diagrams computed for various unsteady mean flows are shown in Fig. 5 for a q^{-3} mean flow, with $\gamma / \varepsilon_0 \xi_0$ varying from 0 (steady flow) to 1 (fast varying flow). The steady mean flow diagram is consistent with the previously discussed ones. The fast varying flow diagram, however, shows a different behavior: the curved boundary present for $\alpha < 1$ had disappeared, and only remains a sharp cutoff at $\alpha = 1$, meaning that frequency shift is always observed for power laws smaller than 1 no matter the initial ratio ε_0 between the RMS of the flow and the group velocity of the waves. This constitutes a white noise regime, in which the variations of the flow are happening so fast that they are decorrelated between each time step, so the waves are seeing very different and abruptly changing features. This is ultimately an analogous regime to the large ε_0 case for the steady flow, in which the group velocity is too small for the waves to follow the flow if $\alpha < 1$. Between the steady and the fast-varying flow cases, a transition occurs for $\gamma / \varepsilon_0 \xi_0 \sim 10^{-2}$, although a precise investigation of this transition was not carried out.
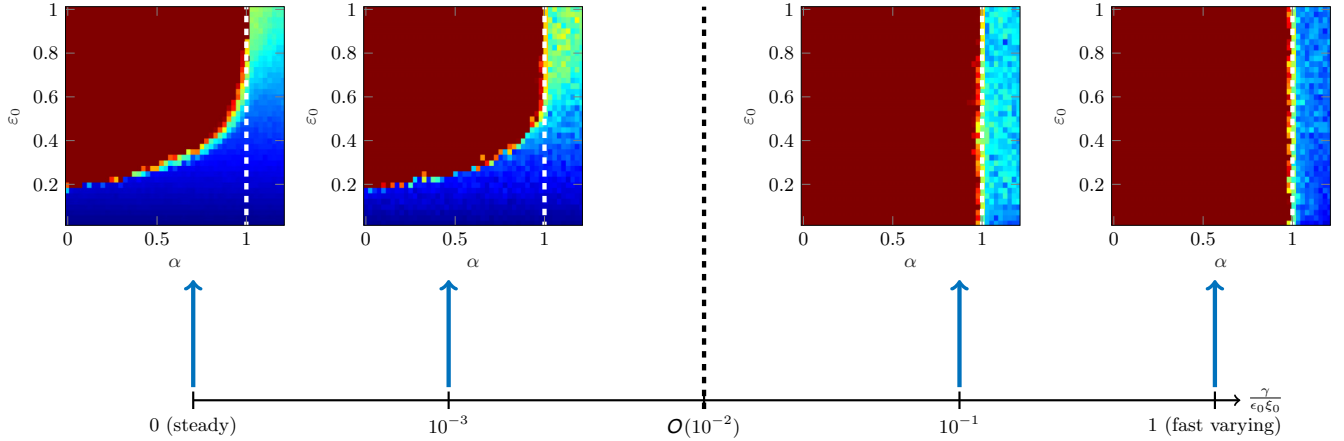
FIG. 5. Evolution of the phase diagram of $\varepsilon(t = 200)$ in the (α, ε_0) space in the case of an unsteady mean flow. On the far left is the base case of a steady mean flow. On the far right is the case of a fast varying mean flow that leads to a decorrelated white noise regime for which the boundary between shift and no-shift is a straight line at $\alpha = 1$. A gradual transition lies in between and separates these two limiting behaviors.

VI. CONCLUDING REMARKS

Motivated by recent studies in geophysical fluid dynamics involving internal and surface gravity waves interacting with a mean flow, we performed detailed ray-tracing simulations of wave packets based on a simple two-dimensional isotropic power-law dispersion relation of the form $\omega \propto k^\alpha$. This model captures some of the pertinent dynamics of internal gravity waves (such as the possible reduction of group velocity with increasing wave number), but it also fails in other respects, which limits that comparison. Foremost of these is that the wavenumber sets belonging to a single frequency are compact circles here while they are unbounded three-dimensional cones for internal waves. So this is a partial analogy at best and our two-dimensional model is more relevant to surface gravity waves.

Now, the ratio ε of the typical mean flow speed U to the group velocity c_g then demarcates two distinct regimes of fast ($\varepsilon \ll 1$) and slow ($\varepsilon \geqslant 1$) waves. The markedly different behavior of these two wave types was illustrated in Fig. 1: fast waves are barely affected by the mean flow, they traverse the domain in a seemingly ergodic fashion, and there is no net drift in their frequency ω. The latter property is particularly important as wave action conservation implies that wave energy changes are proportional to changes in ω, hence fast waves do not exchange much energy with the mean flow. In contrast, slow waves are strongly affected by the mean flow, they get trapped in coherent flow structures such as vortices, and their frequency grows significantly (cf. Figs. 2 and 3), indicating that slow waves are extracting energy from the mean flow.

Fast-slow transitions, whereby a fast wave becomes a slow wave or vice versa, depend on α and on the initial value of ε. Crucially, they also depend strongly on whether the mean flow is steady or not. This is because for steady mean flows the ray-tracing equations conserve the absolute frequency Ω and this conservation in time provides a nontrivial forever link to the initial conditions of the wave packet. The profound implications of this for the long-term dynamics are illustrated in Fig. 4. Clearly, if $\alpha > 1$ then fast waves are the only attracting states in the long run, i.e., fast waves remain fast and slow waves become fast. Alternatively, if $\alpha < 1$ then there is a finite threshold value for ε_0 (depending on α) below which fast waves will remain fast forever; this is the main finding of our study. Above that threshold, on the other hand, fast waves will inevitably transition into slow waves in the long run, thereby limiting the validity in time of asymptotic theories based on fast waves. The underlying mathematical reason for this finite threshold could be illustrated in detail in the special case $\alpha = 1/2$, which is relevant for surface waves.

Now, for unsteady mean flows the conservation of Ω no longer holds and this allows more waves to transition from fast to slow regimes. This is illustrated in the sequence of (α, ε_0) regime diagrams as a function of increased mean flow unsteadiness in Fig. 5: as the unsteadiness increases the thresholding behavior for $\alpha < 1$ gradually fades away until the only remaining regime threshold is $\alpha = 1$. This state of affairs, in which all waves eventually transition to slow waves, is reached already at fairly modest levels of unsteadiness. For example, the third panel corresponds to a rate of change of the mean flow of just 10% of a typical eddy turnover time. From this it seems plausible that in practice sufficient mean flow unsteadiness will be the most likely cause of fast-slow transitions, provided that the dispersion relation links large values of k to small values of c_g.

Of course, our study of unsteady mean flows was restricted to the artificial time evolution of a random stream function pattern, rather than to realistic fluid evolution. In particular, this meant that coherent structures such as vortices did not persist in a Lagrangian fashion in our simulations. Whether this would affect our conclusions requires further study.

ACKNOWLEDGMENTS

[1] M. S. Longuet-Higgins, Longshore currents generated by obliquely incident sea waves: 1, J. Geophys. Res. **75**, 6778 (1970).

[2] D. G. Andrews, J. R. Holton, and C. B. Leovy, *Middle atmosphere dynamics* (Academic Press, New York, 1987).

[3] J. R. Booker and F. P. Bretherton, The critical layer for internal gravity waves in a shear flow, J. Fluid Mech. **27**, 513 (1967).

[4] A. D. Craik, *Wave interactions and fluid flows* (Cambridge University Press, Cambridge, 1988).

[5] O. Bühler, *Waves and mean flows* (Cambridge University Press, Cambridge, 2014).

[6] A. Villas Bôas and W. Young, Directional diffusion of surface gravity wave action by ocean macroturbulence, J. Fluid Mech. **890**, R3 (2020).

[7] H. Kafiabad, M. Savva, and J. Vanneste, Diffusion of inertia-gravity waves by geostrophic turbulence, J. Fluid Mech. **869**, R7 (2019).

[8] M. R. Cox, H. A. Kafiabad, and J. Vanneste, Inertia-gravity-wave diffusion by geostrophic turbulence: The impact of flow time dependence, J. Fluid Mech. **958**, A21 (2023).

[9] M. Savva and J. Vanneste, Scattering of internal tides by barotropic quasigeostrophic flows, J. Fluid Mech. **856**, 504 (2018).

[10] F. P. Bretherton and C. J. R. Garrett, Wavetrains in inhomogeneous moving media, Proc. R. Soc. London A **302**, 529 (1968).

[11] J. Muraschko, M. Fruman, U. Achatz, S. Hickel, and Y. Toledo, On the application of wentzel–kramer–brillouin theory for the simulation of the weakly nonlinear dynamics of gravity waves, J. Roy. Meteorol. Soc. **141**, 676 (2015).

[12] O. Bühler and M. E. McIntyre, Wave capture and wave–vortex duality, J. Fluid Mech. **534**, 67 (2005).

[13] M. Savva, H. Kafiabad, and J. Vanneste, Inertia-gravity-wave scattering by three-dimensional geostrophic turbulence, J. Fluid Mech. **916**, A6 (2021).

[14] W. Dong, O. Bühler, and K. S. Smith, Geostrophic eddies spread near-inertial wave energy to high frequencies, J. Phys. Oceanogr. **53**, 1311 (2023).

[15] C. H. McComas and F. Bretherton, Resonant interaction of oceanic internal waves, J. Geophys. Res. **82**, 1397 (1977).

[16] L. Ryzhik, G. Papanicolaou, and J. Keller, Transport equations for elastic and other waves in random media, Wave Motion **24**, 327 (1996).

[17] W. Dong, O. Bühler, and S. Smith, Frequency diffusion of waves by unsteady flows, J. Fluid Mech. **905**, R3 (2020).

[18] C. Gardiner, *Handbook of Stochastic Methods*, Vol. 3 (Springer, Berlin, 1985).